Modeling, Simulation, and Experimental Verification of a 20-kW Series-Series Wireless Power Transfer System for a Toyota RAV4 Electric Vehicle

Omer C. Onar, Madhu Chinthavali, Steven L. Campbell, Larry E. Seiber, Cliff P. White, and Veda P. Galigekere
Electrical and Electronics Systems Research Division, Power Electronics and Electric Machinery Group
Oak Ridge National Laboratory
National Transportation Research Center, Knoxville, TN USA
onaroc@ornl.gov, chinthavalim@ornl.gov, campbellsl@ornl.gov, seiberle@ornl.gov, whitecp@ornl.gov, galigekerevn@ornl.gov

***Abstract*— Wireless power transfer is going to play a major role in transportation electrification due the convenience, flexibility, safety, and high-efficiency. Achieving high power levels is important in order to reduce the charge times and provide more convenience to electric vehicle (EV) owners while keeping the efficiency high and electric and electromagnetic field emissions lower than the limits set by the international guidelines. This study presents a 20-kW wireless charging system designed for a Toyota RAV4 electric vehicle for stationary charging with a dc-to-dc (high-frequency inverter input to the vehicle battery terminals) efficiency exceeding 95% over four power conversion stages. Additionally, the modeling, analysis, and sensitivity of the wireless charging system are presented for series-series resonant tuning configuration.**

Keywords—Wireless power transfer, electric vehicle, electromagnetic induction resonant, wireless charging.

I. INTRODUCTION

Wireless charging of EVs is deemed as an enabling technology, which is essential for further commercialization of EVs. The advantages of wireless charging of EVs over conventional wired charging are convenience to the consumer resulting from not having to plug in using a heavy cord, safety to the user during inclement weather conditions, and system immunity to dirt, water, pollutants, etc. Wireless charging also has the advantage of being extendable to dynamic vehicle charging easily as compared to wired charging [1], [2].

Starting from the AC grid to the vehicle battery terminals, the system converters must be well designed and operated in order to achieve high efficiency [3]-[5]. In addition, power flow control to the pick-up system should be resolved where the control parameters (DC link voltage, frequency, duty cycle, phase-shift, etc.) should be actively controlled for the improved efficiency while meeting the vehicle side target voltage, current, and/or power. Simultaneously, vehicle side DC link or battery voltage, current, temperature, and the state-of-charge (SOC) should be carefully monitored and fed-back to the primary side for controls and for the start and stop of the charging process. Moreover, the battery management system (BMS) or other vehicle side converters (on-board chargers or dc/dc converters) should be monitored for safety. Typically, there are 4 or 5 power conversion stages in a grid connected system as shown in Fig. 1. Most of these power conversion stages detailed in previous studies. Particularly, reference [6] provides information on high-frequency power inverter, high-frequency isolation transformer, electromagnetic coupling coils, vehicle side rectifier, and the control system while reference [7] introduces various vehicular integration approaches applied to different electric vehicles with different requirements and specifications.

There has been a trend to increase the charging power levels and reducing the charging times in order to have the electrified transportation similar to the conventional transportation system that we have today in terms of the refueling times. Typically, the expectation is to have a charging system with less than 30 minutes of charging time which requires having a high power charger with at least 2 C charging rate applicable to the battery. For instance, an electric vehicle with 10 kWh usable battery energy storage capacity could be charged with 20 kW power to the battery to meet this charging time. For a wireless charging system, existing system limitations include the inverter input and output voltage and current (maximum voltage rating of the inverter devices), high-frequency transformer voltage and current rating without saturation or high core losses, primary and secondary coil wire current rating, primary and secondary tuning capacitor voltage and current rating at the operating frequency, and the vehicle side rectifier voltage and current rating. In order to achieve higher power ratings without exceeding limitations, several methods have been practiced in the literature. Bojarski et al. proposed a three-phase high-frequency inverter with each phase interlinked to each other for higher voltage and current across and through the primary coil using intercell transformers [8]. Using intercell transformers would increase the cost and losses; therefore, using a single set of couplers as in this study is ideal due to eliminated cross-coupling between parallel operating multiple primary and/or secondary couplers.

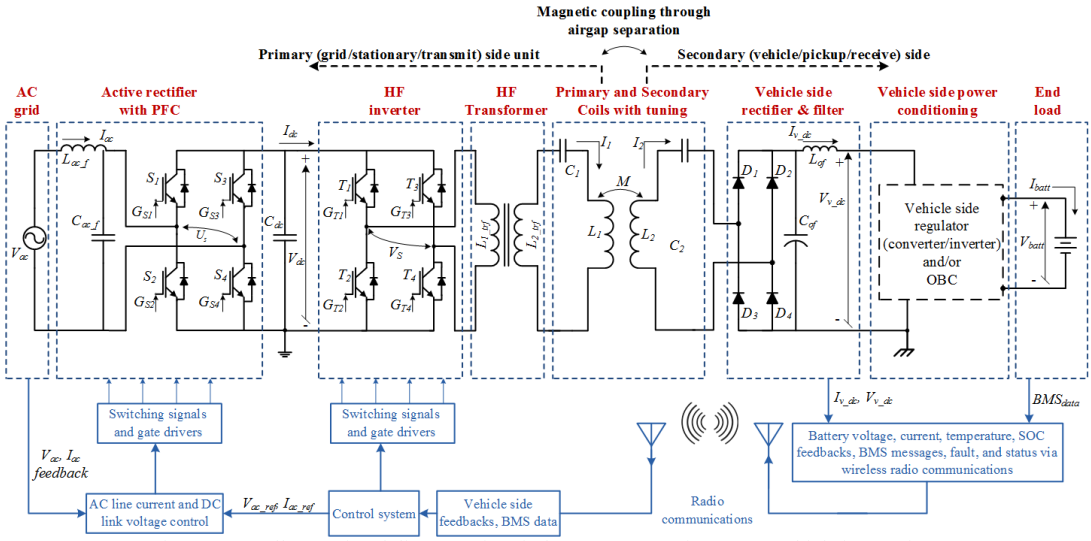

Fig. 1. Overall operational diagram of a wireless power transfer system vehicle integration.

Hao et al. introduced three parallel operating units with each including grid side rectifiers, high-frequency inverters, primary and secondary couplers, and three receiver side rectifiers to improve the power transfer level to about 6 kW while each unit can carry 2 kW each [9]. While this topology provides redundancy; i.e., if one of the parallel units fails, the other two can still transfer reduced power to the load, the complexity is high and there is always a level of cross-coupling among primary coils and secondary coils with other parallel units. In [10], authors paralleled the power electronic devices to increase the current output of the high-frequency inverter where they used three devices in parallel in inverter phase leg high-side and low-side switches. The approach in our study uses high voltage and current power electronic devices in an H-bridge arrangement to reach high power (>20 kW) while using a single primary and secondary coupling coils as given in [6] that readers can refer to.

The other most significant reason for high power wireless charging requirement is for the development of in-motion or also known as "dynamic" wireless charging systems which refers to charging the vehicles while they drive. Since the amount of energy delivered to the vehicle is related to the power rating of the dynamic wireless charging system and the period of time spent on the couplers, power rating has a linear impact on the energy delivery. Considering highway driving speeds (50-70 mph), vehicles only have a few tens of milliseconds to complete the passage over a transmit coil; therefore, it is essential to reach high power levels to improve the energy delivery. Dynamic wireless charging work at Oak Ridge National Laboratory has progressed from charging a small neighborhood electric vehicle manufactured by GEM with 2-transmit coils [11] to a 6-transmit coil system with reduced power pulsations [12], [13].

II. System Modeling and Analysis

Figure 2 (a) shows the resonant stage of the series-series tuned WPT system where the input is supplied by the output of the high-frequency inverter and output is feeds the equivalent load resistance. The primary and secondary coils are linked via the coupling coefficient k. The high-frequency inverter is operated at a switching frequency f_s and an effective duty cycle D resulting in a fundamental frequency component V_{inv_out} to appear at the input of the primary-side resonant network. Higher order harmonics are not considered in this first harmonic approximation analysis.

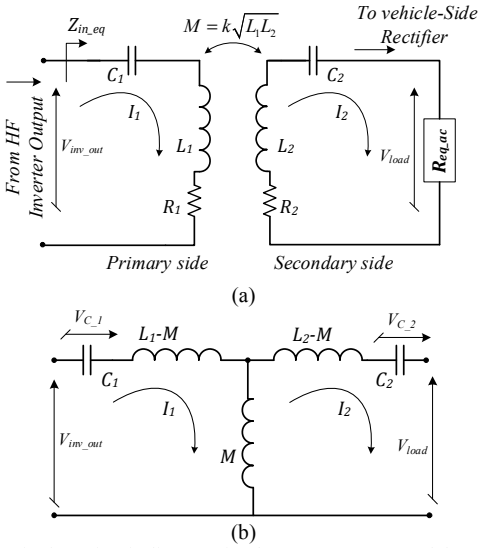

Fig. 2. Equivalent circuit diagram for the WPT system model (a) and the T-equivalent coupled inductor model.

Figure 2 (b) shows the equivalent circuit of the coupled inductor model representing coupling coils. Here, L_1 and L_2 are the self-inductances of the coupling coils, M is the mutual inductance, k is the coupling factor, L_1-M and L_2-M are the primary and secondary leakage inductances, C_1 and C_2 are the resonant tuning capacitors, V_{inv_out} is the inverter output voltage, V_{out} is the output voltage to the rectifier, and I_1 and I_2 are the primary and secondary coil currents. In the loosely coupled transformer model, the magnetizing inductance can be shown by $M = kL_1$, and the leakage inductances of the primary coil is $L_{l1} = (1-k)L_1$, secondary coil is $L_{l2} = (1-k)L_2/n^2$, and the turns ratio of the ideal transformer is $n = \sqrt{\frac{L_2}{L_1}}$ [14].

Both primary and secondary capacitors are chosen to tune out the self-inductance of the transmit and receive side coils [15]-[19] such that:

$$\frac{1}{\sqrt{L_1C_1}} = \frac{1}{\sqrt{L_2C_2}} = 2\pi f_{sw} = \omega_0. \quad (1)$$

The resonant tank is supplied by the high-frequency inverter's output voltage which has three major control parameters as shown in (2). These are; inverter input dc link voltage which can be controlled by the active front-end rectifier, effective duty cycle of the inverter controlled by the phase-shift between the inverter phase-legs, and the switching frequency.

$$V_{out\_inv} = \frac{4V_{dc}}{\pi}\sin\left(\frac{d.\pi}{2}\right)\cos(\omega t). \quad (2)$$

Vehicle side equivalent DC resistance can be written as $R_{dc\_eq} = V_{veh\_dc}/I_{veh\_dc}$ where V_{veh_dc} and I_{veh_dc} are the vehicle side after rectifier voltage and current. Accordingly, resonant tank outpu equivalent AC resistance R_{eq_ac} can be redefined using [20]:

$$R_{ac\_eq} = \frac{V_{veh\_dc}}{I_{veh\_dc}} = R_{dc\_eq} \times \frac{8}{\pi^2}. \quad (3)$$

The power consumed by this equivalent AC resistance of the system is given by [21]

$$P_o = \frac{\omega I_1^2 M^2}{L_2} Q_2 \quad (4)$$

where M is the mutual inductance defined by $M = k\sqrt{L_1L_2}$ where k is the coupling coefficient, and Q_2 is the secondary loaded quality factor (or the inverse voltage boost quality factor [22]) which can be expressed by

$$Q_2 = \frac{\omega L_2}{R_{eq\_ac}} \quad (5)$$

Finally, voltage gain of the system can be defined as [23], [24]:

$$g = \frac{V_{load}}{V_{inv_{out}}}. \quad (6)$$

Using the equivalent ac load resistance and the mutual inductor model shown in Fig. 2 (b), the input voltage to the resonant tank using the circuit parameters and the loop currents can be given as:

$$V_{inv\_out} = \left(R_1 + j\left(\omega_0 L_1 - \frac{1}{\omega_0 c1}\right)\right) I_1 - j\omega_0 M I_2 \quad (7)$$

while voltage loop equation for the secondary side is:

$$0 = j\omega_0 M I_1 - \left(R_2 + + R_{eq_{ac}} + j\left(\omega_0 L_2 - \frac{1}{\omega_0 C_2}\right)\right) I_2 . \quad (8)$$

With that, voltage gain equations can be rewritten as:

$$g = \left|j\omega_0 M R_{eq_{ac}}\right| / \left|\omega_0^2 M^2 + R_1(R_2 + R_{eq_{ac}}) - \left(\omega_0 L_1 - \frac{1}{\omega_0 C_1}\right)\left(\omega_0 L_2 - \frac{1}{\omega_0 C_2}\right) + j\left(R_1\left(\omega_0 L_2 - \frac{1}{\omega_0 C_2}\right) + (R_2 + R_{eq_{ac}})\left(\omega_0 L_1 - \frac{1}{\omega_0 C_1}\right)\right)\right| \quad (9)$$

Based on this WPT model, the system can be characterized in terms of coupling factor, input voltage, load power, switching frequency, and phase and magnitude of the system equivalent impedance seen by the inverter, and the voltage gain.

In addition to (4), the output power of a WPT system can also expressed by [1]:

$$P_o = \omega I_1^2 k^2 L_1 Q_2 \quad (10)$$

In (10), variation in coupling coefficient k can occur because of misalignment due to parking inconsistency or changes in ground clearance due to variation in tire pressure or vehicle load. Variation in quality factor Q_2 occurs due to change in load. To meet the required output power P_o despite changes in k and Q_2, the primary coil current I_1 and/or the coupling frequency ω needs to be changed. Frequency ω and input voltage V_{inv_out}, which control the primary coil current I_1, can be considered system inputs that are varied to regulate power output against variation in k and Q_2. To envisage a control mechanism for the WPT system, it is imperative to analyze the sensitivity of P_o of the WPT system to variation in k, ω, R_L, and V_1.

Consider a WPT system with a matched coil pair having k_{nom}=0.265, L_1=L_2=108 µH, operating frequency f=22 kHz, and envisaged to transfer a rated power of 20 kW V_{dc}=424 V, and $V_{inv,out}$=384 V for a 90% equivalent inverter duty cycle, respectively. With a 5:4 turns ratio step-down transformer, the RMS voltage applied to the resonant network is approximately 300 V. The output voltage is 380.95 V at the vehicle side; therefore equivalent DC resistance at the output is 7.21 Ω with the AC equivalent resistance of 5.85 Ω. The range of k for the analysis is $0.2 \leq k \leq 0.5$, including the nominal value of the k_{nom}=0.265 at the nominal airgap of z=162 mm of the Toyota RAV4 EV. Both for primary and secondary, tuning capacitors of C_1=C_2=0.45 µF are used. Once the initial design is selected, the sensitivity of the circuit to variation in load resistance k and coupling coefficient R_L can be analyzed using Fig. 2. and equations (1) through (11).

Figure 3 shows the total equivalent system impedance of the resonant network. At the nominal coupling factor, this impedance determines the power transfer to the load. At higher coupling factors, this impedance increases which reduces the overall power transfer. The impedance phase angle variation is given in Fig. 4 where the phase angle is zero at the resonant frequency and very close to zero around the resonant frequency. One of the key features that can be inferred from Fig. 4 is that the system has coupling factor independent impedance phase angle which also results in the same phase angle behavior at the inverter output current. This feature ensures the inverter zero-voltage-switching (ZVS) regardless of the coupling factor. Inverter output current, which is also the input current to the system, is presented in Fig. 5. At very low k values, the mutual inductance at the magnetizing branch is also small. Therefore, the primary coil current increases due to this lower impedance path. At resonant, this input current is 83.16 A which is slightly different from the experimental value of 71.18 A. This is due to the fact that component non-

idealities, internal resistances, wire and connector resistances limit input current in the actual physical system.

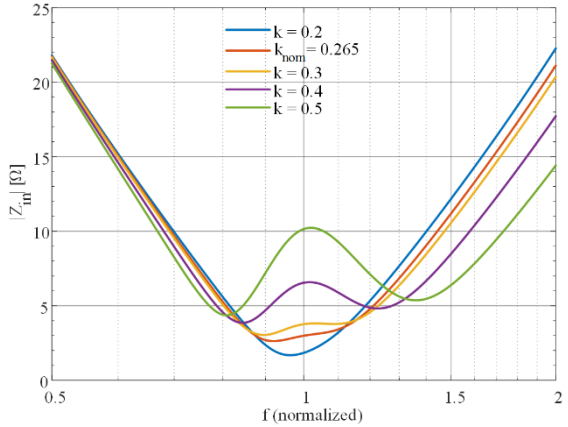

Fig. 3. Magnitude of the system input impedance vs. frequency.

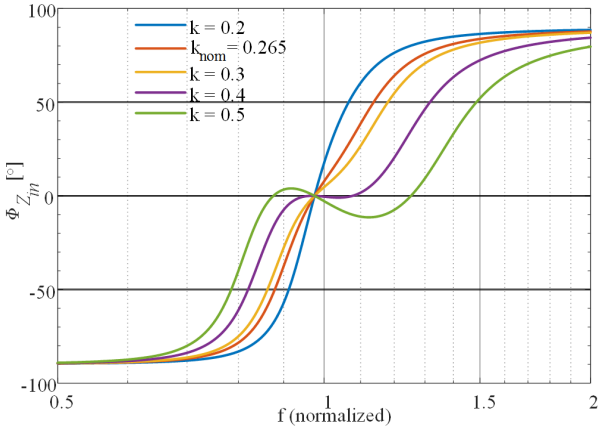

Fig. 4. Phase angle of the system input impedance vs. frequency.

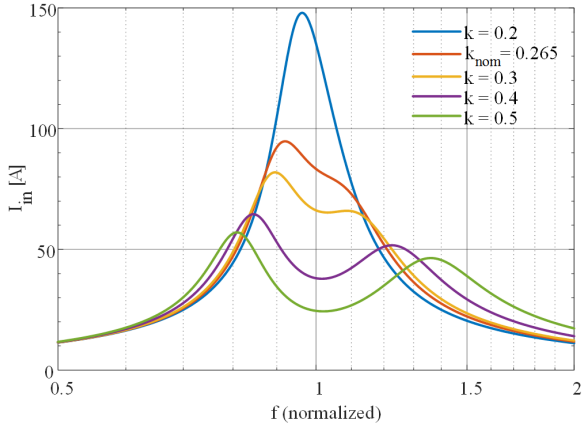

Fig. 5. Input (primary coil / inverter output) current of the system vs. frequency.

The phase angle of the inverter output current is also at or near zero as shown in Fig. 6. This phase angle has the same values with the impedance phase angle but it is 180° shifted or in reverse phase since the voltage has the reference zero angle phase. At the nominal airgap at 20 kW power transfer, experimental data indicates 19.41° of phase angle which is close enough to zero to achieve near ZVS operation. At nominal airgap for 20 kW power transfer, the primary coil current is within the limits of the maximum current rating of the 2 AWG litz wire at ~20 kHz switching frequency.

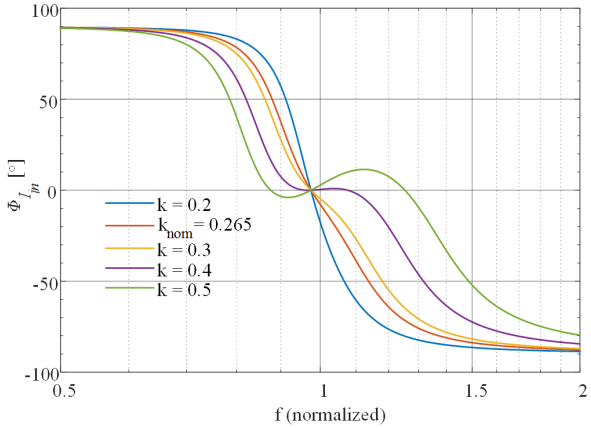

Fig. 6. Phase angle of the input (primary coil / inverter output) current of the system vs. frequency.

Secondary coil current variation with respect to the frequency at different coupling factors is given in Fig. 7. At resonant frequency, the secondary coil current reads 57.17 A at nominal airgap in the sensitivity analysis model whereas the experimental data shows 58.27 A which also verifies the model. Additionally note that the secondary coil peaks at resonant frequency for loosely coupled case. At higher coupling factor values, since the primary coil current is relatively smaller, the secondary side voltage is also smaller resulting in less current on the secondary side. At lower coupling factor values, since the primary current is higher, secondary voltage and current are also higher.

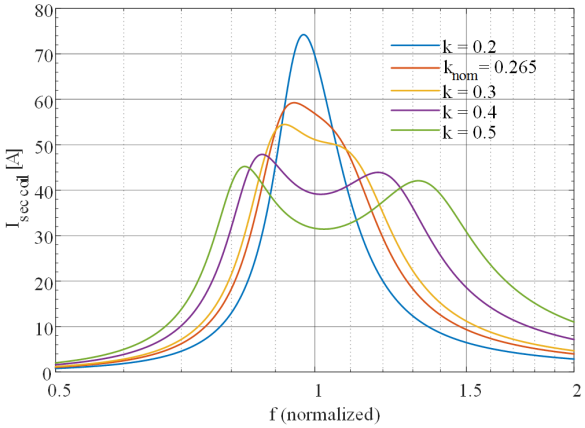

Fig. 7. Phase angle of the input (primary coil / inverter output) current of the system vs. frequency.

In Fig. 8, the output power variation with respect to the frequency is shown at different coupling factors. At nominal airgap and resonant frequency, the total output power is about 20.50 kW whereas the experimental setup showed 20.12 kW. These two values agree with each other and demonstrate the model validity. As shown in Fig. 8 and earlier figures, at high coupling factor, the system impedance is higher due to the relatively larger magnetizing inductance; hence the power transfer is limited. In series-series or series-parallel tuned systems, it is typical to get higher power transfer at smaller

coupling factor values as long as the component limitations (voltage across the tuning capacitors, coil current, etc.) are not exceeded.

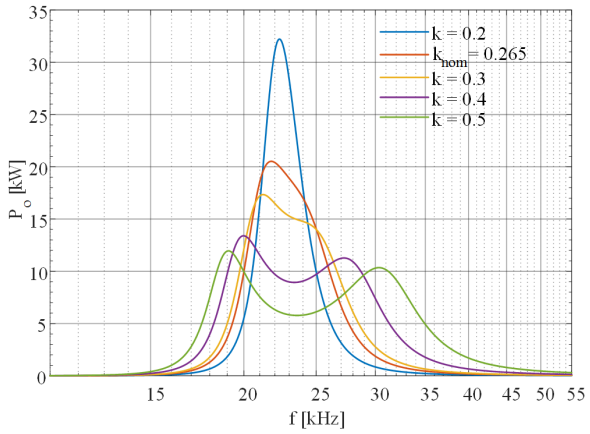

Fig. 8. Output power of the system vs. frequency.

Finally, the voltage and current gain of the system are given in Fig. 9 (a) and (b), respectively. At resonant frequency, nominal airgap, and 20 kW power transfer conditions, the voltage gain is 1.3 and current gain is 0.7 according to the sensitivity analysis model results. In experiments, these ratios were found to be 1.25 and 0.8 which are very close to the model results.

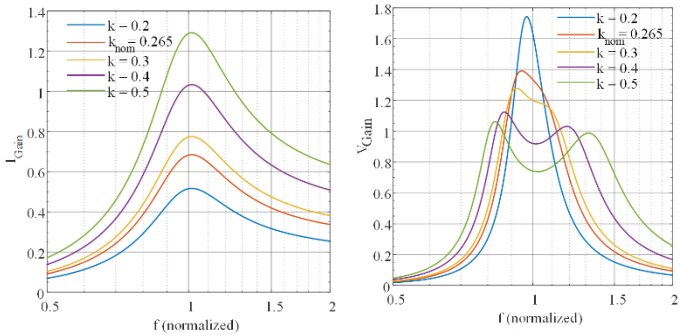

(a) (b)

Fig. 9. Voltage and current gains of the resonant network.

Regarding the isolation transformer shown in Fig. 1, although the resonant coil system separated with an airgap can be considered as a loosely coupled transformer that inherently provides isolation through the large airgap, an additional transformer after the high-frequency inverter is utilized. While providing an additional layer of safety by isolating the primary coil from the grid, if designed in step-down function, this transformer enables inverter to be operated at higher voltage and lower currents that results in less conduction losses and higher efficiencies for the inverter. This transformer is also used for overall voltage matching between the inverter dc input voltage and the vehicle battery voltage keeping in mind the voltage gain of the resonant coupling stage. With 600V/600A Powerex PM600DV1A060 IGBT modules used in this study, inverter is usually more efficient with around 400-450V input voltages. Therefore, at different rated output power levels, the system efficiency can be optimized by adjusting the transformer turns ratio. In other words, adjusting transformer turns ratio allows increasing the primary coil current hence the output power while keeping the inverter input voltage below its limit (usually <450 V for 600 V rated devices). Since the transformer is a closely coupled transformer, the leakage inductance is much smaller than the coil inductance; therefore, its effect on the overall system behavior can be ignored and it can simply be used as a voltage conversion ratio in the models.

III. Experimental Setup and Test Results

Wireless power transfer system integrated Toyota RAV4 vehicle is shown in Fig. 10. A ramp platform that is equipped with two transmit coils is built in authors' laboratory for the experiments. The system parameters are given in Table I.

TABLE I. System Parameters

Parameter	*Symbol*	*Value*	*Unit*
Inverter DC input voltage (variable)	U_{do}	417.67-438.58	[V_{dc}]
Primary tuning capacitor	C_1	0.44	[μF]
Primary coil inductance	L_1	108.2	[μH]
L_1 internal resistance	R_{L1}	37.9	[mΩ]
Secondary coil inductance	L_2	108.2	[μH]
L_2 internal resistance	R_{L2}	37.9	[mΩ]
Secondary tuning capacitor	C_2	0.44	[μF]
Coupling factor	k	0.262	#
Magnetic airgap	z	162	[mm]
Vehicle side filtering capacitor	C_{of}	680	[μF]
Switching frequency	f_s	21-24	[kHz]
Transformer turns ratio (variable)	n	9:3 to 4:3	[#]

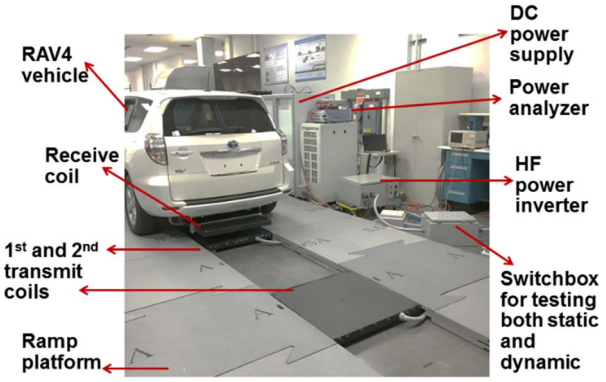

Fig. 10. Stationary and dynamic wireless power transfer laboratory test setup.

TABLE II. Transformer Turns Ratio Impact

XFRM turns ratio [#]	Inverter input voltage [V]	Primary coil current [A]	Primary capacitor voltage [V]	Load power [kW]
9:3	437	62.43	921.69	9.015
7:3	442.56	65.48	966.77	12.034
6:3	438.58	67.43	995.50	14.042
5:3	417.67	69.49	1026	16.053
4:3	424.76	71.18	1050.9	20.122

As mentioned earlier, the turns ratio of the transformer is a key design parameter that adjusts the system's maximum rated power without exceeding the system limits. For instance, with a higher step-down ratio on the transformer, inverter input voltage reaches to the maximum level at lower power transfer level whereas a smaller transformer step down ratio allows more power transfer while keeping the input voltage below the limit. In other words, a smaller transformer turns ratio allows higher voltage (without being stepped down too much) applied

to the resonant circuit which results in higher current and higher magnetic field generation with higher output power to the load. To represent this relationship, the transformer turns ratio, inverter input voltage, primary coil current, and the load power are compiled in Table II. This feature of the transformer turns ratio and the maximum power, allows the system designer to optimize the system for a target load power (the power that system reaches at 400-450V input voltage). With this feature, even the light load efficiency can be high if the system is optimized for that target power. Similarly, when the system is set to higher power, light-load efficiency drops but efficiency at rated power increases. Power vs. dc-to-dc efficiency for different target power levels are shown in Fig. 11. As seen in Fig. 11, regardless of the target rated power, dc-to-dc efficiency can reach up to ~95%. For a system designed for rated power of 20 kW (with 4:3 transformer ratio), light-load efficiency, i.e., efficiency at 3 kW can be as low as 87.6%. However, for a system designed for 9 kW, (with 9:3 transformer ratio), efficiency at the same power output (3 kW) can be as high as 91%. As another example, system with 9 kW rated power is 95% efficient at 9kW; however, system with 20 kW rated power is only ~93.5% efficient at 9 kW output.

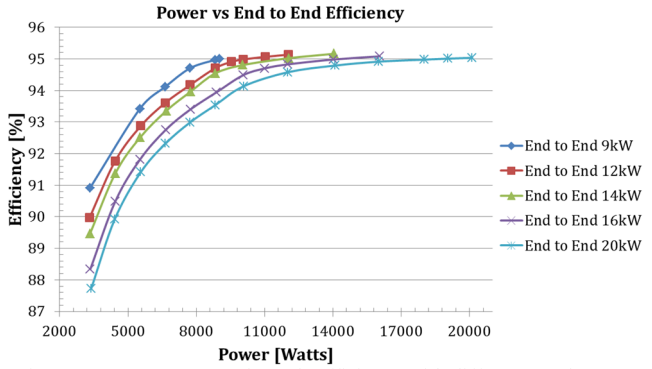

Fig. 11. Output power vs. dc-to-dc efficiency with different rated output power levels set by the transforemr turns ratio.

In Fig. 12, the power vs. efficiency of the system power stages are shown when the system is optimized for 20kW power transfer.

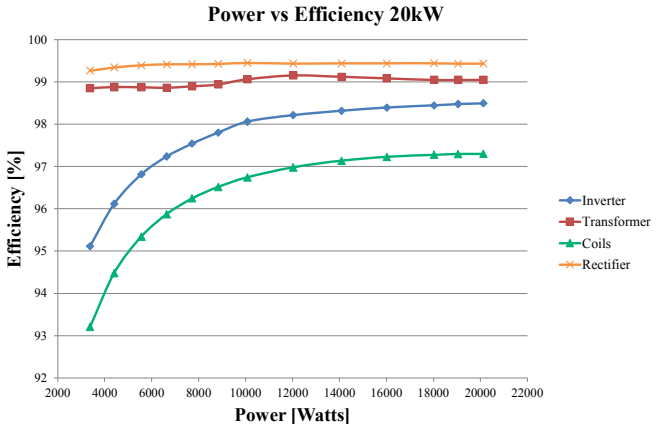

Fig. 12. Power output vs. efficiency of power stages when the system is optimized for 20 kW power transfer.

According to this figure, it is observed that the efficiencies of the high frequency transformer and the vehicle side rectifier are independent to the load power; however, the efficiencies of the inverter and the coupling coils increase with the load power and reaches to maximum at the rated power. This is due to the fact that the transformer is tightly coupled and is a highly efficient transformer while higher power improves the efficiency of the inverter (operating closer to the rated power of the inverter) as well as the coupling coils (higher current provides better coupling for this coil dimensions for this application).

Detailed stage-by-stage power flow, efficiency and the overall efficiency of the system for 20 kW power transfer is provided in Fig. 13. According to this figure, all of the power conversion stages are more than 98% efficient while the coil-to-coil efficiency is ~97.3% although it is at its highest. This relatively lower efficiency is mostly due to the relatively high current on primary and secondary coils (~74 A and ~60 A, respectively) which results in higher I^2R copper losses on the coils.

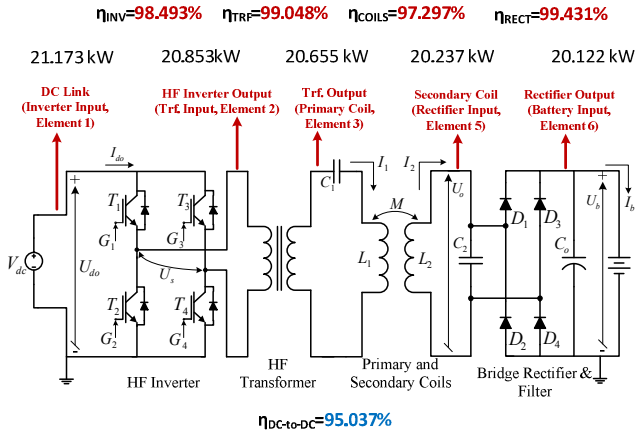

Fig. 13. Stage-by-stage power flow and efficiencies for 20 kW power transfer.

In Fig. 14, the voltage, current, power, power factor, and phase angle measurements for the 20 kW case are displayed. All these values are comparable with the sensitivity model and analysis discussed in Section II.

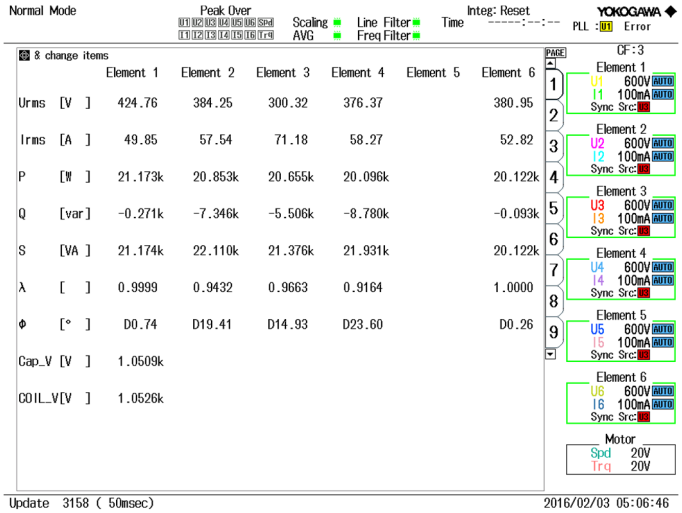

Fig. 14. Voltage, current, power, power factor, and phase angle at all power stages for 20 kW power transfer.

IV. Conclusions

This paper introduces a 20 kW wireless power transfer system integrated into a Toyota RAV4 electric vehicle. A time-domain model was built to analyze system sensitivity and

frequency response. The model developed at resonant frequency and at 20 kW power transfer closely matches the experimental results which verifies the model. The impact of transformer turns ratio on the rated power was analyzed. The dc-to-dc efficiency of the system is shown to be more than 95% including the efficiencies of the high-frequency power inverter, isolation transformer, coupling coils, and the vehicle side rectifier and filter circuit.

REFERENCES

[1] J. M. Miller, O. C. Onar, and M. Chinthavali, "Primary-side power flow control of wireless power transfer for electric vehicle charging," *IEEE Journal of Emerging and Selected Topics in Power Electronics*, vol. 3, no. 1, pp. 147-162, March 2015.

[2] O. C. Onar, J. M. Miller, S. L. Campbell, C. Coomer, C. P. White, and L. E. Seiber, "Oak Ridge National Laboratory Wireless Power Transfer System Development for Sustainable Campus Inititative," in *Proc., IEEE Transportation Electrification Conference and Expo (ITEC)*, pp. 1-8, June 2013, Dearborn, MI.

[3] L. Tang, M. Chinthavali, O. C. Onar, S. Campbell ,and J. M. Miller, "SiC MOSFET based single phase active boost rectifier with power factor correction for wireless power transfer applications," in *Proc., IEEE Applied Power Electronics Conference and Exposition (APEC)*, pp. 1669-1675, March 2014, Fort Worth, TX.

[4] M. Chinthavali, O. C. Onar, S. Campbell, and L. M. Lotbert, "Isolated wired and wireless battery charger with integrated boost converter for PEV applications," in *Proc., IEEE Energy Conversion Congress and Exposition (ECCE)*, pp. 607-614, September 2015, Montreal, Canada.

[5] M. Chinthavali, O. C. Onar, S. Campbell, and L. M. Lotbert, "Integrated charger with wireless charging and boost functions for PHEV and EV applications," in *Proc., IEEE Transportation Electrification Conference and Expo (ITEC)*, pp. 1-8, June 2015, Dearborn, MI.

[6] O. C. Onar, S. L. Campbell, L. Seiber, C. P. White, and M. Chinthavali, "A high-power wireless charging system development and integration for a Toyota RAV4 Electric Vehicle," in *Proc., IEEE Transportation Electrification Conference and Expo (ITEC'16)*, June 2016, Dearborn, MI.

[7] O. C. Onar, S. L. Campbell, L. Seiber, C. P. White, and M. Chinthavali, "Vehicular integration of wireless power transfer systems and hardware interoperability case studies," in *Proc., IEEE Energy Conversion Congress amd Exposition (ECCE'16)*, September 2016, Milwaukee, WI.

[8] M. Bojarski, E. Asa, K. Colak, and D. Czarkowski, "A 25 kW industrial prototype wireless electric vehicle charger," in *Proc., IEEE Applied Poweer Electronics Conference and Exposition (APEC'16)*, March 2016, Long Beach, CA.

[9] H. Hao, G. A. Covic, and J. T. Boys, "A parallel topology for industive power trnsfer power supplies," *IEEE Transactions on Power Electronics*, vol. 29, no. 3, pp. 1140-1151, March 2014.

[10] R. Bosshard and J. W. Kolar, "All-SiC 9.5 kW/dm^3 on-board power electronics for 50kW / 85 kHz automotive IPT system," *IEEE Journal of Emerging and Selected Topics in Power Electronics*, vol. 5, no. 1, pp. 419-431. March 2017.

[11] O. C. Onar, J. M. Miller, S. L. Campbell, C. Coomer, C. P. White, and L. E. Seiber, "A novel wireless power transfer for in-motion EV/PHEV charging," in *Proc., Applied Power Electronics Conference and Exposition (APEC'13)*, pp. 3073– 3080, March 2013, Long Beach, CA.

[12] J. M. Miller, O. C. Onar, C. P. White, S. Campbell, C. Coomer, L. Seiber, R. Sepe, and A. Steyerl, "Demonstrating Dynamic Wireless Charging of an Electric Vehicle: The Benefit of Electrochemical Capacitor Smoothing," *IEEE Power Electronics Magazine*, vol. 1, no. 1, pp. 12-24, March 2014.

[13] J. M. Miller, P. T. Jones, J. M. Li, and O. C. Onar, "ORNL Experience and Challenges Facing Dynamic Wireless Power Charging of EVs," *IEEE Circuits and Systems Magazine*, vol. 15, no. 2, pp. 40–53, May 2015.

[14] F. A. Witulski, "Introduction to modeling of transformers and coupled inductors", *IEEE Transactions on Power Electronics*, vol. 10, no. 3, pp. 349 – 357, 1995.

[15] J. M. Miller, C. P. White, O. C. Onar, and P. M. Ryan, "Grid side regulation of wireless power charging of plug-in electric vehicles," in *Proc., IEEE Energy Conversion Congress and Exposition (ECCE)*, pp. 261-268, September 2012, Raleigh, NC.

[16] Y. Jiang, Y. Wamg, J. Liu, X. Hu, S. Yin, Z. Wang, and L. Wang, "An optimal parameters design methodology of series-series resonant tank of wireless power transmission system for battery charging," in *Proc., IEEE Applied Power Electronics Conference and Exposition (APEC)*, March 2017, Tampa, FL.

[17] C. Fang, J. Song, L. Lin, and Y. Wang, "Practical considerations of series-series and series-parallel compensation topologies in wireelss power transfer application," in *Proc, IEEE PELS Workshop on Emerging Technologies: Wireless Power Tansfer (WoW)*, May 2017, Chongqing, China.

[18] A. A. S. Mohamed, A. Berzoy, F. G. N. de Almeida, and O. Mohammed, "Modeling and assessment analysis of various compensation topologies in bidirectional IWPT system for EV applications," *Transactions on Industry Applications*, vol. 53, no. 5, pp. 4973-4984, September/October 2017.

[19] V. Ravikiran and R. K. Keshri, "Comparative evaluation of S-S and P-S topologies for wireless charging of electrical vehicles," in *Proc., 43rd Annual Conference of the IEEE Industrial Electronics Society*, October/November 2017, Beijing, China.

[20] H. Wu, A. Gilchrist, K. Sealy, and D. Bronson, "A high efficiency 5 kW inductive charger for EVS using dual side control," *IEEE Transactions on Industrial Informatics*, vol. 8, no. 3, pp. 585–595, August 2012.

[21] G. A. G. A. Covic and J. T. Boys, "Inductive power transfer," *Proceedings of the IEEE*, vol.101, no. 6, pp. 1276 – 1289, Jun. 2013.